Modulation of lateral transport of membrane components by spatial variations in diffusivity and solubility

Anthony de Beus and Josef Eisinger
Department of Physiology and Biophyiscs, Mount Sinai School of Medicine, New York, New York 10029 USA

ABSTRACT The effect of spatially varying diffusivity and solubility on the efficiency of intramembrane transport is investigated by obtaining solutions to the generalized lateral diffusion equation in which both the diffusion coefficient, $D(\mathbf{r})$, and the partition coefficient, $K(\mathbf{r})$, are functions of position. The mean-time-to-capture by a sink, t_c, of particles diffusing in a plane is obtained analytically for the case of a sink surrounded by gradients in $D(\mathbf{r})$ and $K(\mathbf{r})$ with radially symmetrical geometry. It is shown that for particles originating at random locations, t_c is shortened dramatically, if in an annular region around the sink, D and K are significantly greater than in the remainder of the plane. Similarly, a viscous boundary layer surrounding a sink is demonstrated to represent a significant barrier for diffusing particles. To investigate more complex geometries, a finite difference numerical integration method is used and is shown to provide comparable results for t_c with modest computational power. The same method is used to calculate the t_c for particles originating at a source that is joined to the sink by a channel. The increase in the rate with which particles travel from a source to a sink when they are joined by a high diffusivity and/or solubility channel is illustrated by several numerical examples and by graphical representations that show the equilibrium particle density (and hence the effective particle flow) in the presence of different sink, source, and channel combinations. These results are discussed in terms of fluidity domains and other membrane heterogeneities.

INTRODUCTION

The intramembrane transport of molecular species, particularly of proteins, plays an essential role in many functions of the cell. Some examples are the accumulation of acetylcholine receptors in synapse formation, the formation of coated pits in receptor-mediated endocytosis, and the "capping" of cells (Taylor et al., 1971; Bretscher, 1984; Edwards and Frisch, 1976). There exists moreover a growing body of evidence that lipid domains and spatially separated phases can persist in model bilayers and cell membranes (Axelrod, 1983; Haverstick and Glaser, 1988; Rodgers and Glaser, 1991). The strict requirement of all biological membranes for large numbers of specific lipid species also suggests the existence of such membrane features. It is therefore appropriate to investigate if intramembrane transport is purely diffusive, as suggested by the basic fluid mosaic model of the membrane (Singer and Nicolson, 1972), or if spatial variations in membrane diffusivity and solubility guide the Brownian motion of membrane particles toward particular sites (Eisinger and Halperin, 1986). This would imply that membrane structure and composition have heterogeneities, e.g., in protein concentration (Peters and Cherry, 1982; Saxton, 1982; Eisinger et al., 1986), and several new experimental approaches to render them observable have recently become available: one employs quantitative fluorescence microscopy of membranes containing dipyrenyl fluidity probes that have been shown to provide a sensitive measure of local membrane fluidity (Vauhkonen et al., 1990) and another uses small colloidal gold particles whose track is recorded by intensified video microscopy while attached to membrane components (DeBrabander et al., 1991; Lee et al., 1991; Qian et al., 1991).

A few years ago a theoretical basis for this kind of "concerted" lateral diffusion was provided by a solution of a generalized, radially symmetrical diffusion equation in which the diffusion coefficient is not a constant but a spatially varying function, $D(\mathbf{r})$ (Eisinger and Halperin, 1986). The same paper also estimated the effect of position-dependent solubility, expressed as a partition coefficient, $K(\mathbf{r})$, on the transport of the diffusing particles. It was shown that t_c, the mean time-to-capture by a sink of particles originating at random locations in the plane, was greatly reduced when the sink was surrounded by a high diffusivity or solubility domain (Eisinger and Halperin, 1986). The present paper extends these findings in several ways. (*a*) It presents a general closed expression for the same radially symmetrical case in which both $D(\mathbf{r})$ and $K(\mathbf{r})$ have step gradients at the same radius. (*b*) These results are now also derived by a numerical integration method that lends itself to many more geometries. These finite difference calculations provide satisfactory agreement with the analytical solution with even modest computational power. (*c*) The finite difference method is used to investigate how the diffusive transport of particles is accelerated if the region between the particle source and sink is occupied by a high diffusivity (or solubility) channel, illustrating the efficacy of such mechanisms.

The limited number of geometries and parametric values considered in the present paper illustrate a methodology for calculating concerted diffusion effects that may play a significant role in membrane biology. They also provide estimates of how the magnitude of these effects are related to putative (or measured) spatial variations in membrane fluidity.

METHODS

1. Formulation and mathematics of the diffusion problem

A detailed formulation of the diffusion problem for the case of a position-dependent diffusion coefficient, $D(\mathbf{r})$, was presented in a previous paper (Eisinger and Halperin, 1986), hereafter referred to as EH, and is not repeated here. The present paper uses the same approach as EH to solve the lateral diffusion equation with both D and K functions of position.

If $\rho(\mathbf{r})$ is the density of particles diffusing in a plane and $j(\mathbf{r})$ is the average particle current at $\mathbf{r}$, then according to Fick's equation, $\mathbf{j}(\mathbf{r}) = -D\nabla\rho(\mathbf{r})$ (Berg, 1983). If the particles' diffusivity and solubility are position dependent, this equation is modified to read (cf. Eq. 25 in EH).

$$\mathbf{j}(\mathbf{r}) = -D(\mathbf{r})[\nabla\rho(\mathbf{r}) + \rho(\mathbf{r})\nabla\phi(\mathbf{r})] \tag{1}$$

where $\phi(\mathbf{r})$ is a generalized conservative potential function, derived below in terms of the solubility. The form of Eq. 1 is justified by the following considerations. In a closed system and in the absence of sources and sinks, the first term takes into account the spatial variations of the diffusion coefficient, whereas the second term ensures that when the solubility varies in space, the equilibrium density distribution has the form

$$\rho_{eq} = \rho_0 K(\mathbf{r}) \tag{2}$$

where $K(\mathbf{r})$ is the partition coefficient and ρ_0 is any constant. For, with the equilibrium solution given by Eq. 2, $\mathbf{j}(\mathbf{r})$ vanishes everywhere. The second term of Eq. 1 therefore represents an effective force on the particles that produces a drift toward regions of higher solubility that, in the equilibrium state, just cancels the diffusion current resulting from the $\nabla\rho(\mathbf{r})$ term. By making the identification

$$\phi(\mathbf{r}) = \ln\frac{\rho_o}{\rho_{eq}(\mathbf{r})} \equiv -\ln K(\mathbf{r}) \tag{3}$$

it is clear that $\rho(\mathbf{r}) = \rho_{eq}(\mathbf{r})$ is indeed a solution of Eq. 1 for which $\mathbf{j}(\mathbf{r}) = 0$.

Consider next an ensemble of particles confined to a surface bounded by an impermeable boundary, S_2, with area A, and containing within it a perfect sink with boundary S_1 (cf. EH Fig. 2). If, in the region between S_1 and S_2, particles are created at random positions and at a rate of ω per second, then it follows from the conservation of particles that once steady-state conditions are achieved, the mean number of particles is exactly equal to $N_{eq} = \omega t_c$, where t_c is the mean-time-to-capture of the diffusing particles, in seconds. More generally, if $\rho_{eq}(\mathbf{r})$ is the particle density at equilibrium,

$$\omega t_c = \int_A \rho_{eq}(\mathbf{r})\, d^2\mathbf{r} \tag{4}$$

In the remainder of this paper, we arbitrarily set $\omega = 1\ \mathrm{s}^{-1}$ without loss of generality. To determine t_c by use of Eq. 4, one must find the time-independent (steady-state) particle probability density, $\rho_{eq}(\mathbf{r})$, for the diffusion equation with the area A containing sources with a density function $q'(\mathbf{r})$. The conservation of particle number then requires that at all points $\mathbf{r}$,

$$\frac{\partial\rho(\mathbf{r})}{\partial t} = -\nabla\cdot\mathbf{j}(\mathbf{r}) + q'(\mathbf{r}) \tag{5}$$

If the sources are uniformly distributed in A, then $q'(\mathbf{r}) = 1/A$, and since in the steady state the particle distribution is invariant with time, the left side of Eq. 5 vanishes and substituting Eq. 1 into Eq. 5 (with $q(\mathbf{r}) = -q'(\mathbf{r})$),

$$\nabla\cdot[D(\mathbf{r})[\nabla\rho(\mathbf{r}) + \rho(\mathbf{r})\nabla\phi(\mathbf{r})]] = q(\mathbf{r}) \tag{6}$$

yields, on expansion,

$$A(\mathbf{r})\nabla^2\rho(\mathbf{r}) + \mathbf{B}(\mathbf{r})\cdot\nabla\rho(\mathbf{r}) + C(\mathbf{r})\rho(\mathbf{r}) = q(\mathbf{r}) \tag{7}$$

with the following definitions.

$$\begin{aligned} A(\mathbf{r}) &\equiv D(\mathbf{r}) \\ \mathbf{B}(\mathbf{r}) &\equiv D(\mathbf{r})\nabla\phi(\mathbf{r}) + \nabla D(\mathbf{r}) \\ C(\mathbf{r}) &\equiv D(\mathbf{r})\nabla^2\phi(\mathbf{r}) + \nabla D(\mathbf{r})\cdot\nabla\phi(\mathbf{r}) \end{aligned} \tag{8}$$

For the sake of simplicity, the subscript of $\rho_{eq}(\mathbf{r})$ was dropped. By making use of Eq. 3, this partial differential equation in $\rho(\mathbf{r})$ is readily transformed into one in $\rho(\mathbf{r})/K(\mathbf{r})$:

$$\nabla\cdot\left[D(\mathbf{r})K(\mathbf{r})\nabla\left(\frac{\rho(\mathbf{r})}{K(\mathbf{r})}\right)\right] = q(\mathbf{r}) \tag{9}$$

The condition imposed on Eq. 1, that at equilibrium $\mathbf{j}(\mathbf{r}) = 0$ everywhere, therefore has been transformed from a condition of the third kind (also known as Robin's type) to the much simpler Neumann type (Young and Gregory, 1973; Press et al., 1988):

$$\nabla\left(\frac{\rho(\mathbf{r})}{K(\mathbf{r})}\right) = 0 \tag{10}$$

Radially symmetric case

If, as was done in EH, the radially symmetrical case is considered, S_1 and S_2 are circles, and the partial differential Eq. 9 may be rewritten as an ordinary differential equation in polar coordinates:

$$\frac{1}{r}\frac{d}{dr}\left[rD(r)K(r)\frac{d}{dr}\left(\frac{\rho(r)}{K(r)}\right)\right] = q(r) \tag{11}$$

If the circles S_1 and S_2 have radii a and b, respectively, then $q(r) = -1/A = 1/\pi(b^2 - a^2)$. By integrating Eq. 11 three times, making use of the boundary conditions $d(\rho(\mathbf{r})/K(\mathbf{r}))/d\mathbf{r} = 0$ at $r = b$ and $\rho(\mathbf{r}) = 0$ at $r = a$ and substituting in Eq. 4, one obtains

$$t_c = \frac{1}{(b^2 - a^2)}\int_a^b\left[\int_a^r \frac{b^2 - s^2}{sD(s)K(s)}\,ds\right]K(r)r\,dr \tag{12}$$

The analytical solution of Eq. 12, which gives the mean time-to-capture when $D(\mathbf{r})$ and $K(\mathbf{r})$ are step functions that change value at $r = c$, where $a \le c \le b$, is derived in the Appendix.

2. Numerical solutions of diffusion equation

Although the radially symmetric case of particles diffusing from randomly distributed sources toward a central sink (see Appendix) is very useful in gauging the effect of diffusivity and solubility gradients on transport, other geometries for which no analytical solutions are available may be equally pertinent to intramembrane transport. Fortunately, Eqs. 4 and 6 can be solved by various numerical methods that are applicable to any geometry. The finite difference method (FDM), although not as versatile as the finite element method (FEM) for complicated geometries, is considerably easier to adapt to new problems because of its simplicity; in addition, it lends itself readily to obtaining solutions on microcomputers with limited memory. Since our primary purpose is to illustrate possible membrane transport mechanisms, the

saving in development time and required hardware make FDM our method of choice.

In the FDM, the derivatives of $\rho(\mathbf{r})$ in Eqs. 7 and 9 are replaced by an algebraic (usually linear) combination of local values of $\rho(\mathbf{r})$ divided by a spatial separation. For example, using central differences, $\partial\rho(x, y)/\partial x$ is replaced by $[\rho(x + \Delta x, y) - \rho(x - \Delta x, y)]/2\Delta x$. The definition of the derivative assures us that in the limit where $\Delta x \to 0$, the limit of the central difference formula will be the average of the left and right hand derivatives at (x, y). What makes FDM a practical computational tool is the fact that the finite difference equation provides a reasonable approximation to the derivative as long as Δx is sufficiently small and $\rho(x, y)$ is sufficiently smoooth. More complete discussions of the convergence properties and consistency of the FDM are given elsewhere (Young and Gregory, 1973; Press et al., 1988).

In the example above, the central difference is exact for functions that are linear over the range of $2\Delta x$; similarly, it is possible to form "higher order" finite differences using the assumption of approximate polynomial behavior over some multiple interval of Δx. Once the finite differences have been formed, the problem of solving the partial differential equation becomes one of solving the simultaneous linear equations in $\rho(x + j\Delta x, y + i\Delta y)$, where $j\Delta x$ signifies the addition of j spatial increments of length Δx each. The solution of these equations yields the approximate value of ρ at points i, j. For our problem, it is sufficient to solve for evenly spaced points in a square so that $\Delta x = \Delta y = \Delta$. For more irregular geometries, it is preferable to use the finite element method, in which piecewise continuous polynomials over convex polygons are used to approximate $\rho(\mathbf{r})$.

For a regular square array of ixj grid points, Eqs. 7 or 9 may be replaced by:

$$a_{ij}u_{i+1,j} + b_{ij}u_{i-1,j} + c_{ij}u_{i,j+1} + d_{ij}u_{i,j-1} + e_{ij}u_{ij} = f_{ij} \quad (13)$$

where $u(i, j) = \rho(j\Delta x, i\Delta y)$. Eq. 7 may be rewritten in terms of central differences as

$$a_{ij} = A(x, y) - B_y(x, y)\frac{\Delta}{2} \quad \text{at} \begin{Bmatrix} x = j\Delta \\ y = i\Delta \end{Bmatrix} \quad (14)$$

$$b_{ij} = A(x, y) + B_y(x, y)\frac{\Delta}{2} \quad \text{at} \begin{Bmatrix} x = j\Delta \\ y = i\Delta \end{Bmatrix} \quad (15)$$

$$c_{ij} = A(x, y) + B_x(x, y)\frac{\Delta}{2} \quad \text{at} \begin{Bmatrix} x = j\Delta \\ y = i\Delta \end{Bmatrix} \quad (16)$$

$$d_{ij} = A(x, y) - B_x(x, y)\frac{\Delta}{2} \quad \text{at} \begin{Bmatrix} x = j\Delta \\ y = i\Delta \end{Bmatrix} \quad (17)$$

$$e_{ij} = -4A(x, y) + C(x, y)\Delta^2 \quad \text{at} \begin{Bmatrix} x = j\Delta \\ y = i\Delta \end{Bmatrix} \quad (18)$$

$$f_{ij} = q(x, y)\Delta^2 \quad \text{at} \begin{Bmatrix} x = j\Delta \\ y = i\Delta \end{Bmatrix} \quad (19)$$

where $B_x(x, y)$, $B_y(x, y)$ are the x and y components of the vector function $\mathbf{B}(x, y)$.

The formulation above presents two problems: if the diffusivity and solubility functions $D(\mathbf{r})$ and $\phi(\mathbf{r})$ are not well behaved (corresponding, say, to adjoining membrane domains of two different lipid phases), then the functions $A(x, y)$, $\mathbf{B}(x, y)$, and $C(x, y)$ are not defined everywhere in the plane. This problem is circumvented by defining the necessary derivatives of D and ϕ at each i, j using a central difference formula at the cost of possibly ill conditioning the problem by overflow for small Δ. The second problem arises from the e_{ij} term. For the simultaneous equations (13) to be solvable by iterative techniques, it is generally necessary to have $e_{ij} \leq 0$ for stability purposes. For arbitrary $D(\mathbf{r})$ and $\phi(\mathbf{r})$, this condition is not met. Even if the simultaneous equations are solved directly using Gaussian elimination, the ill conditioning caused by both of these problems will render solutions impossible except for uselessly large Δ.

It was our experience that the straightforward application of FDM is unsuccessful in solving Eq. 7 because of the discontinuous nature of $D(\mathbf{r})$ and $\phi(\mathbf{r})$, but most of all, of $\rho(\mathbf{r})$! On the other hand, if Eq. 13 is solved with the following definitions,

$$a_{ij} = D\left(x, y - \frac{\Delta}{2}\right)K\left(x, y - \frac{\Delta}{2}\right);$$

$$b_{ij} = D\left(x, y + \frac{\Delta}{2}\right)K\left(x, y + \frac{\Delta}{2}\right)$$

$$c_{ij} = D\left(x + \frac{\Delta}{2}, y\right)K\left(x + \frac{\Delta}{2}, y\right);$$

$$d_{ij} = D\left(x - \frac{\Delta}{2}, y\right)K\left(x - \frac{\Delta}{2}, y\right)$$

$$e_{ij} = -(a_{ij} + b_{ij} + c_{ij} + d_{ij}); \quad f_{ij} = q(x, y)\Delta^2 \quad (20)$$

and $u(i, j) = \rho(j\Delta x, i\Delta y)/K(j\Delta x, i\Delta y)$, in accordance with Eq. 9, then the set of finite difference equations for $u(i, j)$, corresponding to Eq. 13, are well-conditioned, because $u(\mathbf{r})$ is continuous although $\rho(\mathbf{r})$ is not. To integrate the result over the area according to Eq. 5, the average of all the i, j points is taken, weighted by $K(\mathbf{r})$.

A number of general methods for solving Eq. 13 exist in preprogrammed form. Since we are interested in implementing a solution to this equation conveniently and on commonly available microcomputers, the popular simultaneous Over Relaxation Method (Young and Gregory, 1973; Press et al., 1988) was adapted to our iterative method. Routines for the Gaussian elimination method are provided elsewhere (Smith and Griffiths, 1988). These are often used in the FEM, but are readily adaptable to the FDM used here, although for an $N \times N$ square mesh, the computer memory required for them grows as N^3 (rather than N^2 for SOR) with N.

RESULTS

1. Sink surrounded by step gradients in diffusivity and solubility

The case of particles created randomly in a plane and diffusing to a sink surrounded by a circular step gradient in D was solved in EH (Eisinger and Halperin, 1986), where it is shown that the mean time-to-capture, t_c, of the particles in the annular region $a < r < b$ is given by

$$t_c = \frac{1}{b^2 - a^2}\left\{\frac{1}{D_o}\left[\frac{b^4}{2}\ln\frac{b}{c} + \frac{b^4 - c^4}{8} - \frac{b^2(b^2 - c^2)}{2}\right]\right.$$
$$\left. + \frac{1}{D_i}\left[\frac{b^4}{2}\ln\frac{c}{a} + \frac{c^4 - a^4}{8} - \frac{b^2(c^2 - a^2)}{2}\right]\right\} \quad (21)$$

where D_i and D_o are the diffusivities inside and outside the step gradient at $r = c$, respectively, with $a < c < b$ (c.f. Fig. 1). This equation is now extended to include different solubilities, K_i and K_o, in the inner and outer annular

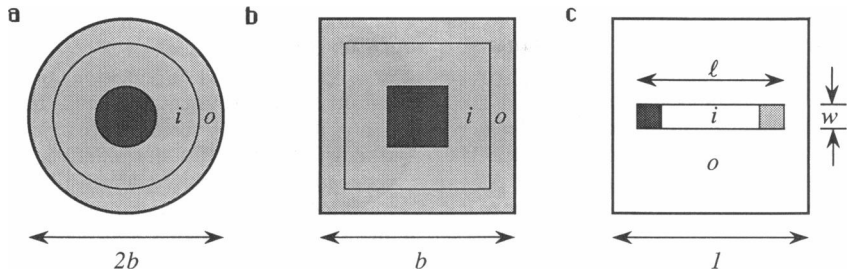

FIGURE 1 Geometrical configurations used for calculating the mean time-to-capture (t_c) of particles originating at random locations and diffusing in the presence of sinks and sources, indicated by heavy and light stippling, respectively. Perfectly reflecting boundaries are shown as heavy lines and step gradients appear as fine lines, with i and o indicating the inner and outer regions, respectively. (a) The radially symmetric case with sink, step gradient, and outer boundary having radii a, c, and b, respectively. (b) The square geometry used to calculate t_c by FDM. The sides of the sink, gradient, and boundary are $2a$, $2c$, and $2b$, respectively. (c) A square sink and square source in a unit square, joined by a diffusivity and/or solubility channel of length (l) (including source and sink) and width (w), inside a unit square (cf. Tables 1 and 3).

regions, respectively. The ratio of the partition coefficients for the two domains is therefore K_i/K_o, and for D and K step gradients at $r = c$ it is shown in the Appendix that

$$t_c = \frac{1}{b^2 - a^2}\left\{\frac{1}{D_o}\left[\frac{b^4}{2}\ln\frac{b}{c} + \frac{b^4 - c^4}{8} - \frac{b^2(b^2 - c^2)}{2}\right] + \frac{1}{D_i}\frac{K_o}{K_i}\left[\frac{b^4}{2}\ln\frac{c}{a} + \frac{c^4 - a^4}{8} - \frac{b^2(c^2 - a^2)}{2}\right] + \frac{1}{D_i}\left(1 - \frac{K_o}{K_i}\right)\left[\frac{b^2c^2}{2}\ln\frac{c}{a} + \frac{c^4 - a^4}{8} - \frac{(b^2 + c^2)(c^2 - a^2)}{4}\right]\right\} \quad (22)$$

This equation gives the average time-to-capture of particles originating in both the inner and outer regions and partitioning between them according to K_i/K_o. It consists of two terms, the first being a function of the particles' diffusivity in the outer region only, whereas the second depends on the partition coefficient and the diffusivity in the inner region, the relative contributions of the two terms being a function only of a, b, and c.

To demonstrate the effectiveness of diffusivity and solubility gradients in accelerating transport to a trap, Eq. 22 was used to evaluate t_c for several parametric values and geometries, with the results shown in Table 1. In the cases considered there, the step gradients in $D(\mathbf{r})$ and $K(\mathbf{r})$ are both located at $c = (a + b)/2$, and t_c values are given for $b/a = 2$ and 10. t_c is given in seconds if D is expressed in units of (length)^2/s, the length units being irrelevant as long as they are identical with those used for the radii a, b, and c.

The values that D can adopt in membrane domains are not well known, but are of the order of 1 μm^2/s for lipid analogue membrane probes. For at least one bilayer (dimiristoylphosphatidylcholine) the long-range (FPR) diffusion coefficient is two or more orders in magnitude greater in the fluid (disordered) than in the gel (ordered) phase (Smith and McConnell, 1978; Alecio et al., 1982; Lotta et al., 1988). Lateral diffusivity of membrane components can also be modulated by the local density of membrane proteins, which can reduce diffusivity by orders of magnitude at moderately high levels (Eisinger et al., 1986; Saxton, 1982).

Table 1 also presents the results of finite difference calculations of t_c for the analogous cases, using square, instead of circular traps, gradients, and boundaries, to facilitate the use of a rectangular grid.

As pointed out above, we chose to use FDM to solve the transport problem in the presence of spatially varying D and K for heuristic reasons, in that a background in elementary calculus is sufficient for the derivation and implementation of the method. Whenever the geometri-

TABLE 1 Mean time-to-capture, t_c, for particles diffusing in a plane in the presence of step gradients in diffusivity and solubility at $c = (a + b)/2$

			$a = 0.25, b = 0.5$		$a = 0.05, b = 0.5$	
K_i/K_o	D_i	D_o	t_c(anal.)	t_c(FDM)	t_c(anal.)	t_c(FDM)
0.1	1	10	0.193	0.171	1.42	1.87
	1	1	0.190	0.177	1.43	1.90
	10	1	0.022	0.022	0.158	0.216
1	1	10	0.026	0.024	0.183	0.244
	1	**1**	**0.030**	**0.029**	**0.197**	**0.270**
	10	1	0.006	0.006	0.034	0.047
10	1	10	0.010	0.010	0.059	0.082
	1	1	0.013	0.013	0.074	0.102
	10	1	0.004	0.004	0.022	0.029

t_c(anal.) values for the radially symmetric geometry (cf. Fig. 1) that appear in columns 4 and 6 were derived from the analytical expression, Eq. 22. The outer and inner annular regions have areas in the ratio of ~3:1 for both b/a ratios for both cases. Columns 5 and 7 give t_c as calculated by FDM for particles diffusing in a unit square and capture by a central square trap in the presence of square step gradients as shown in Fig. 1. The values of t_c in the absence of D and K gradients serve as reference and are shown in bold type. The FDM calculations were performed on a square grid of 161 × 161 points.

TABLE 2 t_c values for the case of $a = 0.25$ and $c = (a + b)/2$ calculated for both the circular and square cases by the FEM

			$a = 0.25, b = 0.5$	
K_i/K_o	D_i	D_o	t_c(circ.)	t_c(sqre.)
0.1	1	10	0.203	0.216
	1	1	0.205	0.223
	10	1	0.024	0.028
1	1	10	0.026	0.029
	1	**1**	**0.030**	**0.034**
	10	1	0.006	0.007
10	1	10	0.009	0.010
	1	1	0.012	0.014
	10	1	0.004	0.005

A comparison with Table 1 shows that there is good agreement between the analytical and FEM values for the circular geometry and between the FDM and FEM values for the square geometry. The FEM calculations used a 45° sector of the planar region, using 324 triangular elements with a total of 190 nodes.

cal boundaries do not coincide with the rectangular mesh, however, FDM becomes rather inefficient to program, and it is for that reason we chose square sources and sinks in solving the case of a rectangular channel connecting them in a square membrane region. Unfortunately, the choice of FDM precluded direct comparison between analytic and numerical solutions for the circular case in Table 1. The FEM (Press et al., 1988), by contrast, is readily adaptable to any geometry, but is considerably more difficult for the novice to understand or implement. Therefore, to verify our FDM accuracy, we obtained solutions for both the circular and square trap problems using the FEM; in fact, the only difference between the circular and square cases in the numerical implementation is that the grid points (for a triangular mesh) for the circular case are given by ($r \cos \theta$, $r \sin \theta$), whereas in the square case, they are (r, $r \tan \theta$), for $0 < \theta < \pi/4$. The results are shown in Table 2. We validated the FEM circular geometry case by comparison with the analytic solution; since the FEM square geometry solution was generated by the same program except for the single change mentioned above, we have confidence in its accuracy. The agreement between the FEM and FDM solutions of Table 2 may therefore be considered a validation of the FDM program.

From the examples of Table 1, certain general conclusions regarding lateral transport to a trap surrounded by D and/or K gradients can be drawn. (a) In the absence of a solubility gradient, t_c is shortened considerably when the trap is surrounded by a high diffusivity domain (large D_i), but only marginally by an increase in D_o. (b) In the absence of a diffusivity gradient, transport to the trap can be slowed severely by reduced partioning into the inner region, whereas partioning into the inner domain produces a limited shortening in t_c. (c) The greatest reduction in t_c is obtained when both diffusivity and solubility are high in the domain surrounding the sink.

To visualize the transport of particles it is useful to prepare a three-dimensional plot of $\rho_{eq}(\mathbf{r})$, the equilibrium particle density for particles diffusing in the plane, as in Fig. 2. Since according to Fick's Law the particle current is proportional to the derivative of $\rho_{eq}(\mathbf{r})$, the steepness of the gradient in any direction is a measure of the magnitude and direction of the probability current of the diffusing particles. The particle density is discontinuous at $r = c$, where the solubility is discontinuous, so that the gradient does not exist there and cannot be used as an estimate of transport (cf. Fig. 2 c). Since particles are generated at a rate of 1 s^{-1}, the average number of particles remaining in the field at any time is given by the volume under the $\rho_{eq}(\mathbf{r})$ surface in the plots of Fig. 2, as well as those of Fig. 4.

Sink surrounded by a boundary layer

Since proteins and larger molecular assemblies are often considered to be surrounded by a boundary layer of lipids, the effect of such a layer on t_c is a special case of biological interest. The effect of a boundary layer with a special diffusivity (D_i) but the same solubility (i.e., $K_i = K_o$) for the diffusing particles can readily be estimated by use of Eq. 21 for the radially symmetrical case. For a trap with radius a, surrounded by boundary layers assumed to have radial widths $0.1a$, $0.2a$, and $0.3a$, and t_c was calculated for boundary layer diffusivities (D_i) ranging from 0.01 to 100 times the value (D_o) in the remainder of the plane. The results are shown in Fig. 3 and it can be seen that a viscous boundary layer can increase t_c significantly. A fluid boundary layer has, on the other hand, minimal effect on the capture time, other than increasing the effective size of the sink.

2. Source and sink joined by diffusivity and/or solubility channels

In the preceding section it was verified that for a wide range of parameters, the FDM calculations and exact solutions give very similar results, justifying the use of FDM for geometrical configurations of sources and sinks for which analytical solutions are unavailable.

One case of potential biological interest is the transport of molecules to a sink, not from the surrounding area as above, but from a localized source in the plane. One may then ask, how is the speed of the diffusive transport related to the diffusivity and solubility in the region between source and sink?

Table 3 provides t_c values for several cases, including some in which the channel joining source and sink has low diffusivity and solubility and obstructs the particle transport. The results were obtained by the FDM, as outlined in the Methods section, for several channel dimensions. The equilibrium density distributions for some of these cases are shown in Fig. 4.

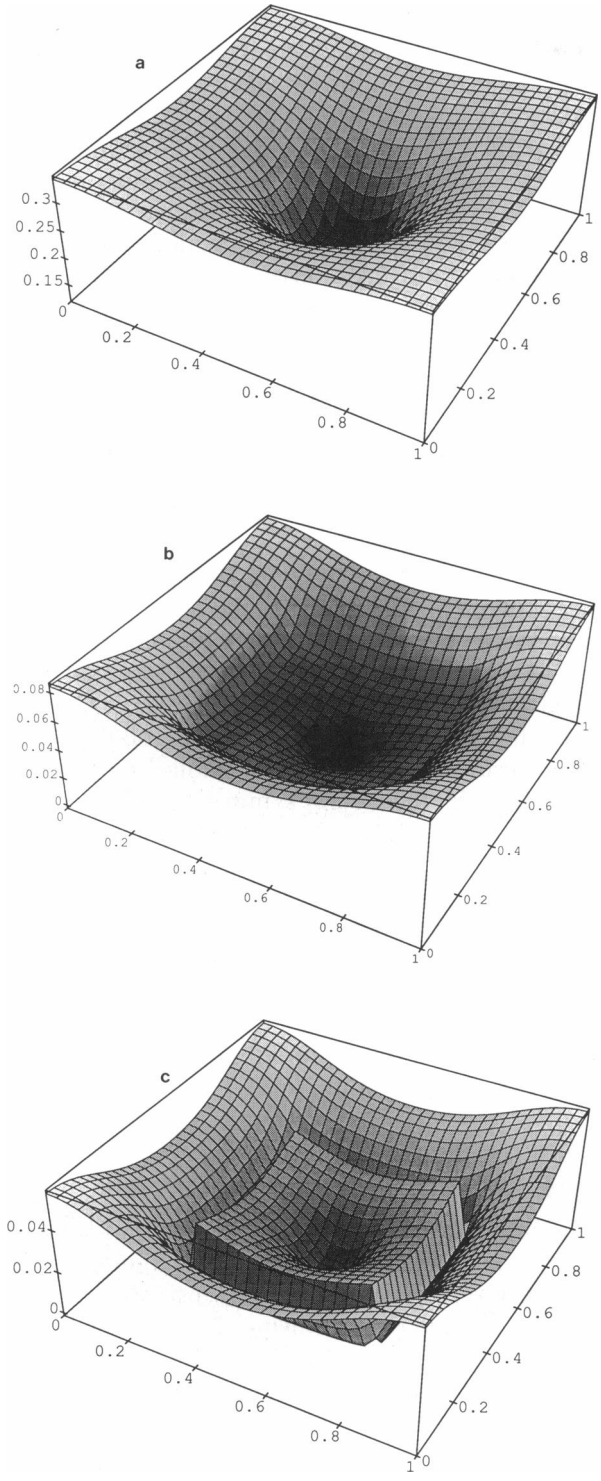

FIGURE 2 Three-dimensional plots of $\rho_{eq}(\mathbf{r})$, the equilibrium density of diffusing particles originating in a unit square with a square sink (side 0.1) surrounded by diffusivity and solubility gradients at a square with sides 0.55. Particles are assumed to be created at random positions at a rate of $\omega = 1\ s^{-1}$, so that the average number of particles at any time is given by the volume of under the $\rho_{eq}(\mathbf{r})$ surface. t_c values for the three cases illustrated in *a*, *b*, and *c* are listed in the 5th column of Table 1. Note that the particle current at $\mathbf{r}$ is proportional to the derivative $\nabla\rho(\mathbf{r})$. (*a*) $D_i = D_o = K_i/K_o = 1$; (*b*) $D_i = 10$, $D_o = 1$, $K_i/K_o = 1$; (*c*) $D_i = 10$, $D_o = 1$, $K_i/K_o = 10$.

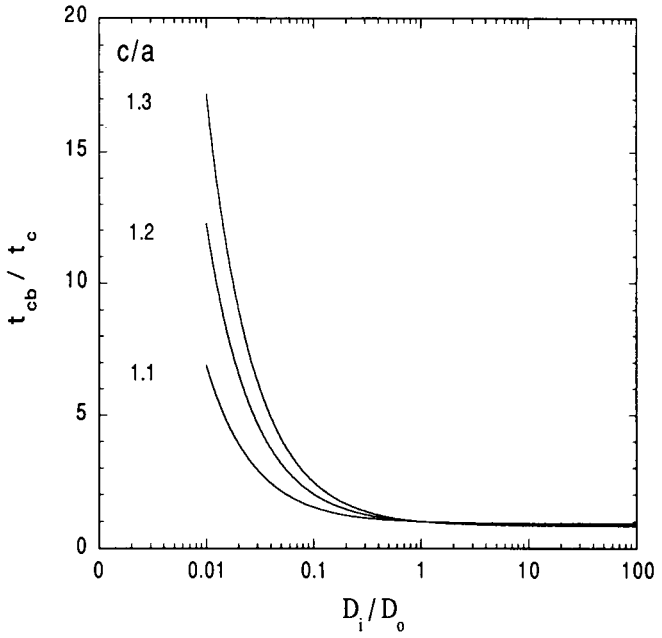

FIGURE 3 The enhancement, t_{cb}/t_c, caused by a boundary layer surrounding a central sink. t_{cb} and t_c are the time-to-capture times in the presence and absence of the boundary layer, respectively. The diffusing particles are confined to a circular area of radius 0.5 (cf. Fig. 1), the sink has radius 0.05, and the boundary layer has radii $c = 1.1a$, $1.2a$, and $1.3a$. The diffusion coefficient in the boundary layer ($a < r < c$) is D_i, and in the remainder of the area $c < r < b$, it is D_o. Note that whereas a relatively viscous boundary layer retards capture by the sink significantly, a relatively fluid boundary layer has a negligible effect.

Note that in the FDM calculations the particles are confined to a square region with reflecting boundaries, and if a boundary is in close proximity to a source or sink, it can alter t_c, compared with the value for an isolated sink, source, and channel in an infinite plane. That this perturbation is not significant in the cases discussed here is seen from a comparison of the t_c values in columns 5 and 7 in Table 3, for which the length/width ratio is the same. For these two cases, the proximal distance from sink (or source) to boundary is 0.25 and 0.375, respectively, and the corresponding sets of t_c values differ by $\sim 10\%$.

Columns 4 and 5 of Table 3 show that, as might be expected, a smaller separation between sink and source leads not only to a shorter t_c but to a greater reduction in t_c when the source and sink are joined by a channel with high diffusivity and/or solubility.

DISCUSSION

The effects of spatially varying membrane diffusivity and solubility on intramembrane transport were investigated by obtaining analytical and numerical solutions to the generalized lateral diffusion equation. The finite difference method was shown to provide good estimates of

TABLE 3 t_c for particles originating at a source joined to a sink by a channel

			t_c			
K_i/K_o	D_i	D_o	$w = 0.062$ $l = 0.25$	$w = 0.062$ $l = 0.5$	$w = 0.031$ $l = 0.5$	$w = 0.031$ $l = 0.25$
0.1	1	10	0.19	0.27	0.41	0.31
	1	1	1.78	2.63	4.03	3.03
	10	1	1.32	2.16	3.49	2.48
1	1	10	0.18	0.27	0.41	0.31
	1	**1**	**1.34**	**2.24**	**3.55**	**2.50**
	10	1	0.40	0.90	1.80	1.01
10	1	10	0.16	0.29	0.42	0.27
	1	1	0.43	1.18	2.12	1.10
	10	1	0.06	0.17	0.38	0.16

From the similarity of t_c values in columns 5 and 7, it is concluded that the "boundary proximity effect" discussed in the text is small. The values of t_c in the absence of a channel serve as reference and are shown in bold type. It is noted that for this case, as for that of Table 1, t_c is inversely proportional to the magnitude of the diffusion coefficients: e.g., if $D_i = 10$ and $D_o = 1$, t_c is 10 times smaller than for the case $D_i = 1$ and $D_o = 0.1$. w and l are the width and length of the channel, respectively.

the average capture times by a sink for particles diffusing in the presence of sources and/or sinks in an arbitrary geometrical configuration. The computer requirements for using the FDM are modest, and estimates of t_c can be obtained for a configuration on a 128 × 128 mesh of lattice points in a few hours, using Simultaneous Over Relaxation and double precision (depending on D and K) on a 80386 microcomputer, equipped with 1.5 MB of memory. By contrast, the FEM calculations (cf. Table 2) were programmed in BASIC (64 Kb memory required) and would require only ~1 h using an 8086/8088 microcomputer or equivalent.

The examples of Tables 1 and 3 and Fig. 3 illustrate the magnitude of concerted diffusion effects resulting from certain kinds of D and K heterogeneities. Although they show that the speed of diffusive transport can be modulated by one or more orders of magnitude by diffusivity and/or solubility gradients, the selectivity of direction of transport that these mechanisms facilitate may be equally important in membrane transport phenomena (cf. Figs. 2 and 4). It was also demonstrated that a viscous (low D) boundary layer surrounding a sink represents a significant barrier for diffusing particles (ligands).

This having been said, it is noted that there exists at this time only sparse compelling evidence either for membrane domains or the concerted diffusion effects they give rise to. However, as pointed out in the Introduction, new experimental techniques based on low light fluorescence imaging (Vauhkonen et al., 1990; DeBrabander et al., 1991) may before long provide the dynamic topographical data with which the significance of these effects can be evaluated.

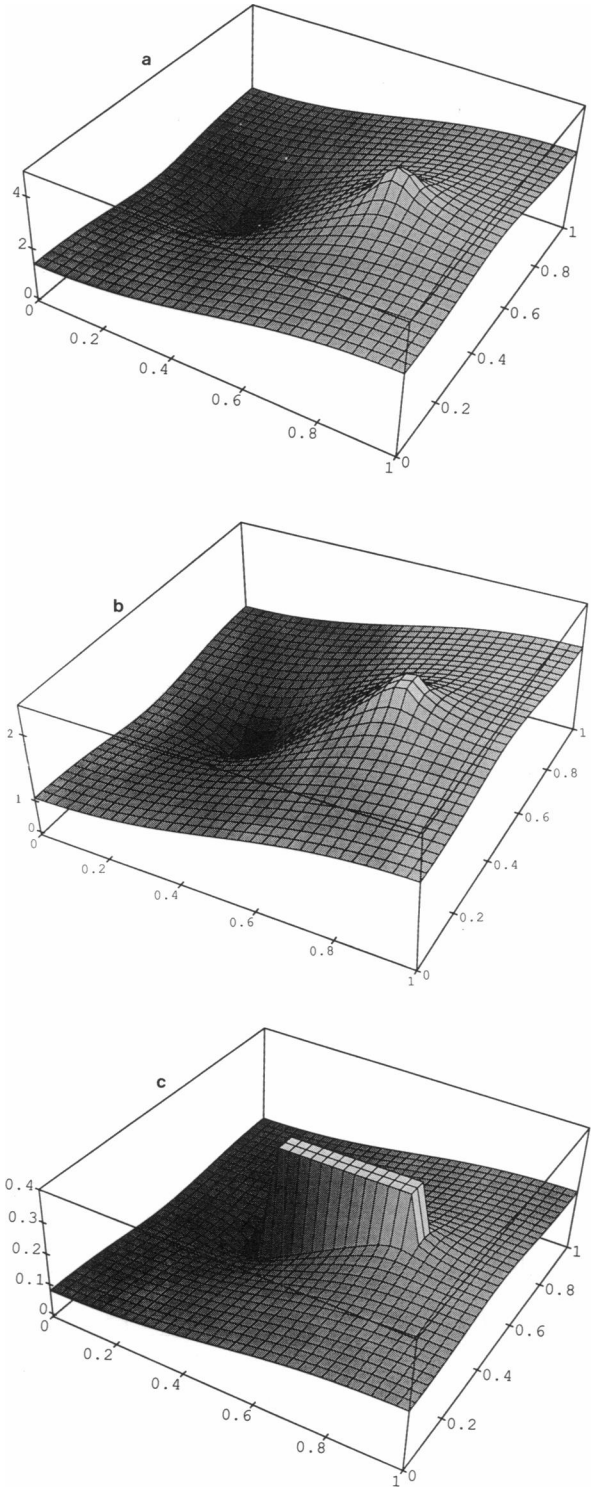

FIGURE 4 Three-dimensional plot of $\rho_{eq}(\mathbf{r})$ for a particle sink and a source, which creates particles at a rate of 1 s^{-1}, joined by a diffusivity and/or solubility channel with dimensions $l = 1/2$, $w = 1/16$ (cf. Fig. 1 *c*). The subscripts i and o refer to the inside and outside of the channel. The t_c values for *a*, *b*, and *c* are shown in the 5th column of Table 3. (*a*) $D_i = D_o = K_i/K_o = 1$; (*b*) $D_i = 10$, $D_o = 1$, $K_i/K_o = 1$; (*c*) $D_i = 10$, $D_o = 1$, $K_i/K_o = 10$. In *c*, $\rho_{eq}(\mathbf{r})$ within the channel rises linearly from sink to source where it has the value of 4.0, but this portion of the plot was truncated at 0.4 in the figure.

APPENDIX

This Appendix presents an analytical solution for the average time-to-capture (t_c) by a circular trap ($r = a$) of particles originating at random locations in the region $a \le r \le b$, in the presence of step gradients in both diffusivity and solubility at $r = c$ ($a < c < b$; cf. Fig. 1). According to Eq. 12,

$$t_c = \frac{1}{(b^2 - a^2)} \int_a^b \left[\int_a^r \frac{b^2 - s^2}{sD(s)K(s)}\, ds \right] K(r) r\, dr \quad \text{(A1)}$$

where the functions $D(\mathbf{r})$ and $K(\mathbf{r})$ are given by

$$D(\mathbf{r}) = \begin{cases} D_i & \text{for } a < r < c \\ D_o & \text{for } c < r < b \end{cases} \quad \text{(A2)}$$

$$K(\mathbf{r}) = \begin{cases} K_i & \text{for } a < r < c \\ K_o & \text{for } c < r < b \end{cases} \quad \text{(A3)}$$

Eq. A1 can be written as the sum of three integrals:

$$t_c = \frac{1}{b^2 - a^2} (I_1 + I_2 + I_3) \quad \text{(A4)}$$

Since in the inner region ($a < r < c$), $D(\mathbf{r})$ and $K(\mathbf{r})$ are constant, it follows from Eqs. A1 and A4 that

$$I_1 = \frac{1}{D_i} \int_a^c \left[\int_a^r \frac{b^2 - s^2}{s}\, ds \right] r\, dr \quad \text{(A5)}$$

$$I_2 = \int_c^b \left[\int_a^c \frac{b^2 - s^2}{sD_iK_i}\, ds \right] K_o r\, dr \quad \text{(A6)}$$

I_2 and I_3 are the integrations over the outer region:

$$I_3 = \int_c^b \left[\int_c^r \frac{b^2 - s^2}{sD_oK_o}\, ds \right] K_o r\, dr \quad \text{(A7)}$$

The integration of I_1 straightforward, with the integrations over the inner and outer regions resulting in the following two equations:

$$\int_a^r \left(\frac{b^2}{s} - s \right) ds = b^2 \ln \frac{r}{a} + \frac{a^2 - r^2}{2} \quad \text{(A8)}$$

$$\int_a^c \left(b^2 r \ln \frac{r}{a} + \frac{a^2 r - r^3}{2} \right) dr = \frac{b^2 c^2}{2} \ln \frac{c}{a} - \frac{c^4 + a^4}{8} + \frac{b^2(a^2 - c^2) + a^2 c^2}{4} \quad \text{(A9)}$$

The inner integration of I_2 is identical with that of I_1 with $r = c$, resulting in a linear integration in r for the outer region:

$$\frac{1}{D_iK_i} \int_a^c \left(\frac{b^2}{s} - s \right) ds = \frac{1}{D_iK_i} \left[b^2 \ln \frac{c}{a} + \frac{a^2 - c^2}{2} \right] \quad \text{(A10)}$$

$$K_o \int_c^b \frac{1}{D_iK_i} \left[b^2 \ln \frac{c}{a} + \frac{a^2 - c^2}{2} \right] r\, dr = \frac{K_o}{D_iK_i} \left[b^2 \ln \frac{c}{a} + \frac{a^2 - c^2}{2} \right] \left[\frac{b^2 - c^2}{2} \right] \quad \text{(A11)}$$

The third integral I_3 is similar to I_1, with the inner and outer integrations giving the following two expressions:

$$\frac{1}{D_oK_o} \int_c^r \left(\frac{b^2}{s} - s \right) ds = \frac{1}{D_oK_o} \left[b^2 \ln \frac{r}{c} + \frac{c^2 - r^2}{2} \right] \quad \text{(A12)}$$

$$\frac{1}{D_o} \int_c^b \left(b^2 r \ln \frac{r}{c} + \frac{c^2 r - r^3}{2} \right) dr = \frac{1}{D_o} \left[\frac{b^4}{2} \ln \frac{b}{c} + \frac{b^4 - c^4}{8} - \frac{b^2(b^2 - c^2)}{2} \right] \quad \text{(A13)}$$

Combining the three integrals Eqs. 8–13 according to Eq. A4 and rearranging the terms yields Eq. 20 in Results above.

This work was supported by National Institutes of Health grants 1R24 RR-05272 and HL-21016.

Received for publication 27 November 1991 and in final form 30 April 1992.

REFERENCES

Alecio, M. R., D. E. Golan, W. R. Veatch, and R. R. Rando. 1982. Use of a fluorescent cholesterol derivative to measure lateral mobility of cholesterol in membranes. *Proc. Natl. Acad. Sci. USA.* 79:5171–5174.

Axelrod, D. 1983. Lateral motion of membrane proteins and biological function. *J. Membr. Biol.* 75:1–10.

Berg, H. C. 1983. Random Walks in Biology. Princeton University Press, Princeton, NJ. 17–36.

Bretscher, M. S. 1984. Endocytosis: Relation to capping and cell locomotion. *Science (Wash. DC).* 224:681–686.

DeBrabander, M., R. Nuydens, A. Ishihara, B. Holifield, K. Jacobson, and H. Geerts. 1991. Lateral diffusion and retrograde movements of individual cell surface components on single motile cells observed with nanovid microscopy. *J. Cell. Biol.* 112:111–124.

Edwards, C., and H. L. Frisch. 1976. A model for the localization of acetylcholine receptors at the muscle endplate. *J. Neurobiol.* 7:377–381.

Eisinger, J. and B. I. Halperin. 1986. Effects of spatial variation in membrane diffusibility and solubility on the lateral transport of membrane components. *Biophys. J.* 50:513–521.

Eisinger, J., J. Flores, and W. P. Petersen. 1986. A milling crowd model for local and long-range obstructed lateral diffusion. Mobility of excimeric probes in the membrane of intact erythrocytes. *Biophys. J.* 49:987–1001.

Haverstick, D. M., and M. Glaser. 1988. Visualization of domain formation in the inner and outer leaflets of a phospholipid bilayer. *J. Cell Biol.* 106:1885–1896.

Lee, G. M., A Ishihara, and K. A. Jacobson. 1991. Direct observation of Brownian motion of lipids in a membrane. *Proc. Natl. Acad. Sci. USA.* 88:6274–6278.

Lotta, T. I., J. A. Virtanen, and P. K. J. Kinnunen. 1988. Fourier transform infrared study on the thermotropic behaviour of fully hydrated 1-palmitoyl-2-[10-(pyren-1-yl)decanoyl]sn-glycero-3-phosphatidylcholine. *Chem. Phys. Lipids.* 46:13–23.

Peters, R., and R. J. Cherry. 1982. Lateral and rotational diffusion of bacteriorhodopsin in lipid bilayers: experimental test of the Saffman-Delbruck equations. *Proc. Natl. Acad. Sci. USA.* 79:4317–4321.

Press, W. H., B. P. Flannery, S. A. Teukolsky, and W. T. Vetterling,

1988. Numerical Recipes in C. The Art of Scientific Computing. Cambridge University Press, Cambridge.

Qian, H., M. P. Sheetz, and E. L. Elson. 1991. Single particle tracking. Analysis of diffusion and flow in two-dimensional systems. *Biophys. J.* 60:910–921.

Rodgers, W., and M. Glaser. 1991. Characterization of lipid domains in erythrocyte membranes. *Proc. Natl. Acad. Sci. USA.* 88: 1364–1368.

Saxton, M. J. 1982. Lateral diffusion in an archipelago. Effects of impermeable patches on diffusion in a cell membrane. *Biophys. J.* 39:165–173.

Singer, S. J., and G. L. Nicolson. 1972. The fluid mosaic model of the structure of cell membranes. *Science (Wash. DC).* 175:720–731.

Smith, B. A., and H. M. McConnell. 1978. Determination of molecular motion in membranes using periodic pattern bleaching. *Proc. Natl. Acad. Sci. USA.* 75:2759–2763.

Smith, I. M., and D. V. Griffiths. 1988. Programming the Finite Element Method. John Wiley & Sons, New York. 239–249.

Taylor, R. B., P. H. Duffus, M. C. Raff, and S. de Petris. 1971. Redistribution and pinocytosis of lymphocyte surface immunoglobulin molecules induced by anti-immunoglobulin antibody. *Nature New Biol.* 233:225–229.

Vauhkonen, M., M. Sassaroli, P. Somerharju, and J. Eisinger. 1990. Dipyrenyl phosphatidylcholines as membrane fluidity probes. Relationship between intramolecular and intermolecular excimer formation rates. *Biophys. J.* 57:291–300.

Young, D. M., and R. T. Gregory. 1973. A Survey of Numerical Mathematics. Vol. II. Addison-Wesley, New York. 951–1074.